Landscape and Urban Planning 125 (2014) 117–129

Contents lists available at ScienceDirect

Landscape and Urban Planning

journal homepage: www.elsevier.com/locate/landurbplan

Research Paper

How factors of land use/land cover, building configuration, and adjacent heat sources and sinks explain Urban Heat Islands in Chicago

Paul Coseo*, Larissa Larsen[1]

Urban and Regional Planning, University of Michigan at Ann Arbor, 2000 Bonisteel Boulevard, Ann Arbor, MI 48109, United States

HIGHLIGHTS

- Combined fourteen physical measures to estimate elevated air temperatures.
- Determined that nighttime and daytime UHIs are driven by different variables.
- Higher daytime winds make nighttime UHIs easier to predict than daytime UHIs.
- Identified waste heat's significant role in increasing daytime temperatures.

ARTICLE INFO

Article history:
Received 2 July 2013
Received in revised form 10 February 2014
Accepted 17 February 2014
Available online 12 March 2014

Keywords:
Urban Heat Island
Vulnerability
Urban planning
Mitigation
Neighborhoods

ABSTRACT

Urban Heat Islands (UHI) are urban and suburban areas with elevated surface and air temperatures relative to surrounding rural areas. This study combines variables from the remote sensing and urban climatology publications to explain UHI intensity in eight Chicago neighborhoods. During the summer of 2010, we collected air temperature measurements within an urban block in each neighborhood. Consistent with remote sensing research that measures surface temperature, the predictors of elevated nighttime air temperatures were land cover variables. At 2 a.m., the urban block's percentages of impervious surface and tree canopy explained 68% of the variation in air temperature. At 2 a.m., the other physical measures of urban canyon and street orientation were not significant. At 2 a.m. during extreme heat events, the urban block's percentages of impervious surface and tree canopy explained 91% of the variation in air temperature. At 4 p.m., the only significant explanatory variable was distance to industrial sites and this explained 26% of the variation in air temperature. At 4 p.m. during extreme heat events, there were no significant predictors. We believe this research illustrates the importance of differentiating time of day for residential and non-residential areas in UHI mitigation efforts and the need to include waste heat in future UHI investigations.

1. Introduction

Cities have the ability to modify their climates. These modifications include changing cloud cover, precipitation patterns, wind speeds, solar irradiance, and increasing air temperatures (Oke, Johnson, Steyn, & Watson, 1991; Santamouris, 2001). The most significant modification is the creation of Urban Heat Islands. The term Urban Heat Island (UHI) refers to an urban area with temperatures that are elevated relative to its less developed surroundings. While the physical mechanisms causing UHIs are well documented (Oke, 1987), they continue to be the most studied phenomenon in urban climatology (Johnson et al., 1991; Oke, 1973; Stewart, 2011). One reason for urban climatologists' continued interest is that the known physical mechanisms dynamically interact with each city's contextual characteristics, such as its biophysical features, urban development pattern, local weather patterns, and adjacent water bodies.

Urban planners, urban designers, public health officials, and city decision-makers are increasingly concerned with UHIs as research reveals that urban areas are warming at a faster rate relative to their surrounding rural areas and UHIs amplify heat extremes (Stone, 2012). While planners, designers, and decision-makers want to identify the most significant causes of UHI, most seek a simplified method appropriate for neighborhood-level interventions but one that does not require remote sensing analysis. By combining measures of land use/land cover, building configuration, and adjacent heat sources and sinks that are easily collected, we seek a practical

* Corresponding author. Tel.: +1 734 936 0234.
E-mail addresses: pcoseo@umich.edu (P. Coseo), larissal@umich.Edu (L. Larsen).
[1] Tel.: +1 734 678 3964; fax: +1 734 763 2322.

http://dx.doi.org/10.1016/j.landurbplan.2014.02.019
0169-2046/

set of metrics to understand the key drivers of elevated urban air temperatures.

After a brief discussion of UHIs, we review how factors of land use/land cover, building configuration, and adjacent heat sources and sinks contribute to surface and air UHIs. This review provides the basis for our selection of 14 independent variables of interest. Next, we summarize the contextual characteristics of Chicago, a city in a temperate climate and grassland biome that is adjacent to Lake Michigan. Then we describe our selection of eight Chicago neighborhoods and collection of daytime and nighttime summer weather data. Using regression analysis, we identify the independent variables that explain the largest proportion of the neighborhood air temperature variation by time of day. We repeat this analysis for a heat event. We conclude with a discussion of the results and their contribution to the UHI literature.

While known studies of UHIs date back to Luke Howard's research in London in the early 1800s, the term first emerged in the meteorological literature in the 1940s (Stewart & Oke, 2012). UHIs are not limited to large cities but exist within settlements as small as 1 km^2 (Imhoff, Zhang, Wolfe, & Bounoua, 2010). Although climate change is contributing to rising urban temperatures, Stone (2012) determined that most large US cities are warming twice as fast as the planet. Stone believes that land-use change and waste-heat are contributing more toward this warming than global climate change. No matter the confluence of causes, UHIs will increasingly threaten the liveability and safety of urban environments. While the maximum UHI temperatures occur in late afternoon, public health research has determined that nighttime minimum air temperatures are the strongest predictor of heat-related mortality (Kalkstein & Davis, 1989). Therefore, useful UHI research needs to consider nighttime minimum air temperatures as well as daytime maximums.

Much of the research into UHIs can be coarsely divided into broad scale approaches that use remotely sensed satellite images to locate UHIs by surface temperature and fine-scale approaches that use small weather stations or mobile measurement devices to determine UHIs using air temperatures. Surface temperature variations are greatest during the day but air temperature variations are greatest during the night (Lo & Quattrochi, 2003). In the following section, we begin by highlighting relevant findings from a few remote sensing studies that examine how different land use and land cover variables explain land surface temperature. Then, we transition to finer-scale investigations from urban climatology that measure air temperatures to determine how three-dimensional built configuration and adjacent heat sources and sinks impact the UHIs.

1.1. Land use/land cover

Typically remote sensing studies examine the impacts of land use/land cover changes by examining what percentage of the surface temperature can be explained by the presence of impervious surface (building roofs and pavements), vegetation indices, and surface characteristics such as elevation and topography (Lo & Quattrochi, 2003). Research based on remote sensing has effectively documented both the magnitude and spatial distribution of UHIs across broad regions and the heat trapping properties of many building and paving materials. In the following paragraphs, we highlight some of the key results that have emerged from remote sensing research on the UHI.

Imhoff et al. (2010) used remotely sensed images of 38 of the most populated urban areas within the continental United States to understand the influence of development density, spatial extent of the city, and bioclimatic region on surface temperature. Partitioned into grid cells, each city's urban area was defined by grid cells with more than 25% impervious coverage. Across these 38 US cities in eight bioclimatic regions, the percentage of impervious surface explained approximately 70% of the land surface temperature. Among the cities, the amount of variance explained by the percentage of impervious surface varied from 60 to 90%. The authors concluded that the areas of urban impervious surface explained the extent and intensity of the UHI more accurately than earlier techniques that used the city's total population (Oke, 1973). They also found that the city's surrounding bioclimatic environment influenced the magnitude of the UHI. The magnitude of the UHI was greater (6.5–9 °C) in areas that had displaced forested environments relative to temperate grasslands and savannas (6.3 °C) and tropical grasslands (5 °C). So urban areas in temperate climates may have greater UHI intensity relative to semi-arid and arid areas. While this research confirmed the importance of impervious surface as an important indicator and the influence of ecological context on the UHI's magnitude, Imhoff and colleagues (2010) note that their work does not capture the finer-scale microclimate variations that result from different ecological patterns within cities.

Two earlier remote sensing studies illustrated that UHI are not always concentrated in the urban core and may be dispersed throughout urban and suburban areas. Lo and Quattrochi (2003) published a remote sensing study that examined how land use/land cover changes in the thirteen county Atlanta Metropolitan Area altered the location and intensity of UHIs. The researchers identified six land use/land cover types: high-density urban use (largely commercial and industrial), low-density urban use (largely residential), cultivated or exposed land, cropland or grassland, forest, and water. During the twenty-five year period of rapid city expansion, areas of high-density and low-density land use increased by 90 and 119% respectively while areas of forest and cropland decreased by 21 and 33% respectively. In summer 1987, DeKalb County (near the center) was the hottest county and Cherokee County (northern edge) was the coolest. However, by summer 1997, the hottest county was Gwinnett (northeast edge) and the coolest was Cowetta County (southwest corner). With the changes in land use/land cover in metro Atlanta over a ten year period, the region developed four predominant UHIs (Lo & Quattrochi, 2003). By the late 1990s, suburban areas overtook areas near downtown Atlanta to become the region's warmest locations.

The irregular distribution of the UHI within cities is also related to vegetation and, in some locations, socioeconomic neighborhood patterns. In Phoenix, Arizona, Jenerette et al. (2007) found that temperature differences within the metropolitan area varied systematically with neighborhood-level social characteristics. Poorer neighborhoods were significantly hotter. Every $10,000 increase in neighborhood annual median household income was associated with 0.28 °C decrease in the surface temperature at 10 a.m. on a May morning. A multivariate model using path analysis showed that the cooler temperatures associated with higher income neighborhoods were primarily the result of increased vegetation cover. In this semi-arid location, few plants (native or exotic) self-propagate and in poor neighborhoods, residents generally cannot afford to buy plants or water. While we generally recognize the installation costs of vegetation, writers seldom mention that poorer households in arid and semi-arid locations may not be able to maintain vegetation due to water costs. This study also underscored that the presence of pervious surfaces does not always imply vegetation by default. Most importantly, this study alerts us to the concern that UHIs may disproportionately burden the city's poorest residents.

All types of vegetation are not equally effective in mitigating the UHI. Grass is not as effective as trees that cast shade and contribute more moisture. Stone and Norman (2006) determined that if the suburban areas of Atlanta reduced their lawn areas by 25% and replaced them with trees, they could reduce the contribution of unwanted heat to UHIs by 13%.

Finally, Klock, Zwart, Verhagen, and Mauri (2012) combined remote sensing with measures of the physical environment to investigate the pattern and intensity of surface UHIs in 22 neighborhood districts in Rotterdam, in the Netherlands. The researchers analyzed fifteen remote sensing images taken between 1984 and 2007 and then they calculated five physical characteristics within each district. These physical characteristics were albedo, sky view factor, and percentages of green space, impervious surface, and water surface. Using regression analysis, Klock and colleagues (2012) concluded that amount of green space, impervious surface, and albedo within the district were the most significant physical characteristics. Green space explained 69% of the variance in temperature: for every 10% increase in green area, surface temperature decreased by 1.3 °C. Impervious surface was the second most important predictor: for every 10% increase in impervious area, the surface temperature increased by 0.7 °C. Interestingly, the percentage of water within the district was not a significant predictor but this research did not measure the distance from each district to the adjacent major water bodies. They found that the districts with the most intense UHI varied between nighttime and daytime. The researchers also compared the surface temperatures with air temperatures and determined that surface temperatures explained 81% of air temperatures. They estimated that a surface UHI of 10 °C might equate to an air UHI of 7 °C. Klock and colleagues' study bridging surface temperature with district-level physical characteristics provides us with some important guidance as to the significant physical characteristics, the potential difference in day and nighttime UHI locations, and the relationship of surface and air temperatures.

1.2. Building configuration

The relationship between surface and air temperature is mediated by factors such as surface roughness, wind speed, and wind direction that result from the three dimensional characteristics of building and street configuration (Stathopoulou & Cartalis, 2007, p. 359; Voogt & Oke, 2003; Weng, 2009, p. 340; Weng & Quattrochi, 2006). In addition to spatial variations within the urban landscape, urban microclimates can be vertically divided into two areas. The urban boundary layer is above the building rooftops while the urban canopy layer extends from the building tops to the ground surface (Oke, 1987). It is the air temperatures within the urban canopy that impact human well-being. Researchers have shown that surface and air temperatures are highly correlated under light wind conditions (Bonacquisti, Casale, Palmieri, & Siani, 2006; Djen, Jingchun, & Lin, 1994; Gedzelman et al., 2003; Kim & Baik, 2002; Klysik & Fortuniak, 1999; McPherson et al., 1997; Stewart, 2011). Winds at night tend to be lighter than during the day due to decreased solar heating and less atmospheric mixing. In fact, Klysik and Fortuniak (1999) found that under the lightest winds (0–1 m/s) Urban Heat Islands in Lodz, Poland took on a highly variable multicellular pattern, intensifying the air temperature contrasts between urban areas in relatively close proximity.

Common three-dimensional building characteristics that impact air temperature and may contribute to UHIs are building heights, street width, openness, and street orientation (Eliasson, 1996; Oke, 2004; Sakakibara, 1996). Building heights determine the division between the boundary and canopy layers, solar access, shading, and radiational cooling (Oke, 1987). Generally, higher building heights mean less air circulation and more trapped heat energy in the urban canopy layer and therefore, higher air temperatures.

The urban canyon ratio considers the height of the buildings relative to street width (h/w). During the day, tall buildings with narrow streets increase the retention of solar radiation (as it is absorbed by the building walls) and thereby increase air temperatures. From an urban climate perspective, Oke (1988) suggests an ideal urban canyon ratio of 0.40–0.60 (h/w). Past research has shown that urban canyon ratio is a significant predictor of air temperatures (Eliasson, 1996; Sakakibara, 1996). Oke and colleagues (1991) found that urban canyon ratio and the presence of impermeable surfaces were approximately equal in their contribution to the elevated air temperatures of UHIs.

Sky view factor (SVF) is another measure of a neighborhood's three-dimensional character. Similar to urban canyon ratio, SVF measures the relative amount of unobstructed sky or openness at a particular location. However, unlike the urban canyon ratio, SVF also considers the impact of trees and topography. SVF varies from 0 to 1.0, where 1.0 is 100% unobstructed sky, such as an open flat field without trees. SVF has been found to be an important measure of the potential of a location for radiational cooling (Eliasson, 1996; Svensson, 2004). Svensson (2004) found that SVF readings ranging from 0.34 to 0.98 explained 58% of the variance in air temperatures in the city of Göteborg, Sweden. Chang, Li, and Chang (2007) found that parks with more than 40% lawn areas were actually cooler on summer nights than those with less lawn and more trees because the tree canopies impeded cooling.

Finally, another three-dimensional building configuration measure frequently identified in the urban climatology literature is urban canyon (or street) orientation. The orientation of streets affects shading and air circulation, thus influencing air temperature and UHIs. Ali-Toudert and Mayer (2007) using modeling software found that east–west streets in Ghardaia, Algeria had higher temperatures relative to north–south streets because east–west streets lacked shading over the course of the day. In the same study, the authors also noted that streets that were aligned with the prevailing wind were expected to have lower air temperatures relative to perpendicular streets. Therefore from the literature on urban climatology we have selected the four variables of average building height, urban canyon ratio, SVF, and street orientation.

1.3. Adjacent heat sources and sinks

Finally, we identify seven variables to represent adjacent heat sources, heat sinks, and contextual characteristics. Heat sources and sinks from adjacent areas may impact air temperature as wind transports air from upwind locations. Upwind heat sources play an important role in contributing anthropogenic waste heat to neighborhood microclimates (Britter & Hanna, 2003; Fan & Sailor, 2005; Shashua-Bar & Hoffman, 2000). Research has indicated that anthropogenic heat, such as waste heat from industry, cars, and air conditioning units, increases UHIs by 1–5 °C (Britter & Hanna, 2003; Fan & Sailor, 2005; Shashua-Bar & Hoffman, 2000). Shashua-Bar and Hoffman (2000) found that heavily trafficked streets in Tel-Aviv accounted for up to 2 °C warming. Therefore, upwind industrial and highway locations may increase neighborhood air temperatures.

Upwind heat sinks include vegetated areas. The literature indicates that as an area of vegetation increases in percentage and concentration, its cooling effects are magnified and positively impact adjacent, particularly leeward neighborhoods. Chang et al. (2007) showed that in Taipei City, Taiwan, the largest parks (12 ha or greater) were most effective in consistently providing cooling relief at noon in summer, whereas parks smaller than 2 ha were heat islands. On closer examination, Chang and colleagues found that the smaller parks generally contained more than 50% impervious surface. Similarly, studies in Tel-Aviv, Israel, have shown that a vegetated site measuring 20–60 m in width had a perceivable effect on air temperature from two to four times the width of the site. As a park's size increased in width the distance of its effect increased as well, finding a 2 km wide park had a perceivable impact on air temperatures up to 2 km from the edge of the park

(Shashua-Bar & Hoffman, 2000). Therefore, the distance to industrial areas, highways, and parks are potential variables of interest.

The characteristics of the immediate upwind area can also influence neighborhood air temperatures. While the appropriate size of the upwind area of influence varies within the literature, Oke (2004) suggests that the adjacent area of interest is generally captured by an elliptical shape of 0.5 km in length upwind from a 3-m high sensor. Therefore, characteristics such as the adjacent area's average building height and percentage tree canopy may impact air temperatures.

Many writers comment on the importance of larger contextual features. Because of the concentration of buildings and activities, downtown districts tend to have more waste heat from air conditioning and car traffic particularly in the daytime (Oke, 2006; Stone, 2012). Large water bodies also influence air temperatures. Oswald et al. (2012) found that daily air temperatures in Detroit were highly correlated with the distance to the Detroit River and that locations closer to the city's major river were cooler. Similarly, Ackerman (1985) reported that lake breezes and synoptic cold air advection cooled nearshore areas in Chicago. The distance to the downtown core and large water bodies are also potential independent variables that influence neighborhood air temperature.

1.4. Research questions

This study examines how the physical characteristics of eight neighborhoods in Chicago differentially contribute to elevated air temperatures. Specifically we investigate three research questions. First, which individual physical characteristics explain the greatest proportion of the neighborhood's temperature difference? Second, does the relative importance of the physical characteristics vary by time of day? Third, does the relative importance of the physical characteristics vary during a heat event? Based on the literature, we hypothesize that the land cover/land use variables of the percent impervious surface and tree canopy will be the most important explanatory variables. However, at nighttime, when the wind speeds are lower, we hypothesize that local building configuration variables will be more important than adjacent heat sources and sinks. Conversely, in daytime when wind speeds are higher, we hypothesize that adjacent heat sources and sinks will explain more variance in the air temperature than building configuration. Finally, we believe that extreme heat events will strengthen the existing relationships between the physical characteristics and the neighborhood's air temperature.

2. Methods

2.1. Context

The Chicago region lies on the flat Lake Michigan plain (41° 52′ 55″ North and 087° 37′ 40″ West (USGS$_a$, 2012)) with minimal elevation changes of 176.5 m (579 ft.) to 205.1 m (673 ft.) above sea level (USGS$_b$, 2012). Chicago, Illinois, has a moderate continental climate with an average mean air temperature from May to September of 25.9 °C (1961–1990) (Hayhoe, Sheridan, Kalkstein, & Greene, 2010). In July and August, prevailing west-southwest (240°) winds average 13.2 km/h (8.2 mph) (1981–2010) transporting in warm humid air from the central and southern plains (Angel, 2013). The highest recorded temperature in Chicago was 40.6 °C (105 °F) on July 24, 1934 (NWS Chicago Records, 2012). Tree cover plays an important role in moderating air temperatures in the region. McPherson and colleagues (1997) found that the city of Chicago had an average tree canopy of 11%. Street trees comprised 10% of the total canopy in the city, but contributed 24% of the total leaf surface area for all trees in Chicago. According to Imhoff and colleagues (2010), Chicago falls within a grassland bioclimatic region. Another important contextual factor is Chicago's location on the west side of Lake Michigan (Fig. 1). While this major water body can provide some summertime cooling, the location of the lake downwind from the prominent southwest wind may lessen its effect. The Lake's cooling influence also wanes in late summer when water temperatures can reach as high as 26.7 °C (80 °F).

While the 2010 population of the Chicago-Joliet-Naperville metropolitan statistical area was 9,461,105, the city of Chicago's population was 2,695,598 residents (Fig. 1) (US Census, 2012). In 2010, Chicago had an average population density of 45.7 persons per ha (18.1 persons per acre) within the city limits. Researchers suggest that Chicago's current UHI patterns are likely to intensify with a warming climate and further urbanization in the region (Hayhoe et al., 2010; Vavrus & Van Dorn, 2010).

2.2. Neighborhood selection

We used three criteria to select eight Chicago neighborhoods. First, we used a City of Chicago (2006) study of elevated surface temperatures to select neighborhoods within 305 m (1000 ft.) of an elevated surface temperature area (with one exception explained later). Next, we purposefully selected neighborhoods that varied by household income and by racial characteristics. Third, we selected four east–west oriented streets/alleys (Wicker Park, Little Italy, Austin, and Beverly) and four north–south oriented streets/alleys (Logan Square, Bronzeville, Belmont Cragin, and East Side) to understand how orientation may influence canyon shading and ventilation and thus contribute to air temperatures. Tables 1 and 2 describe each neighborhood's social and physical characteristics grouped by orientation of the alley (east–west or north–south). We had one intentional exception to the selection criteria. We included the neighborhood of Beverly in our analysis. Concerned with using Midway Airport as the baseline condition (Appendix A) the neighborhood of Beverly (while not near a surface UHI area) represented a neighborhood with lower impervious cover and higher tree canopy in the SW portion of the city where prevailing winds are just entering Chicago. Within each neighborhood, we selected one representative city block to record air temperature, relative humidity, and to calculate its physical characteristics.

2.3. Data collection

The dependent variable was the difference in air temperatures between each neighborhood and Midway airport at 2 a.m. (nighttime) and 4 p.m. (daytime). We refer to this difference in air temperature as the *UHI intensity*. We took weather observations in each neighborhood using a stationary Onset U23-002 HOBO External Temperature/RH Data Logger with sensor and a model RS3 solar radiation shield. The HOBO weather stations have an air temperature accuracy of ±0.2 °C from 0 to 50 °C (Onset, 2012). We followed Oke's criteria (2004) to establish the locations and heights of the measurement units in the neighborhoods. Each HOBO station was mounted on the north or east side of a utility pole with two screws and two zip ties to secure the station at a height of 3 m (above the height of truck traffic) at the center of each neighborhood block's alley. The units were located within the urban canopy layer as residential building heights were a minimum of 9.14 m. We collected ambient air temperature and relative humidity every 5 min for 24 h a day from July 1 to August 31, 2010. Data were downloaded every two weeks using a HOBO data shuttle to transfer the data from each weather station to a laptop computer. Additional hourly weather observations from July 1 to August 31, 2010 were obtained from Midway Airport, Chicago. Data from Midway Airport was used to calculate baseline air temperature, wind speed and direction, and sky condition.

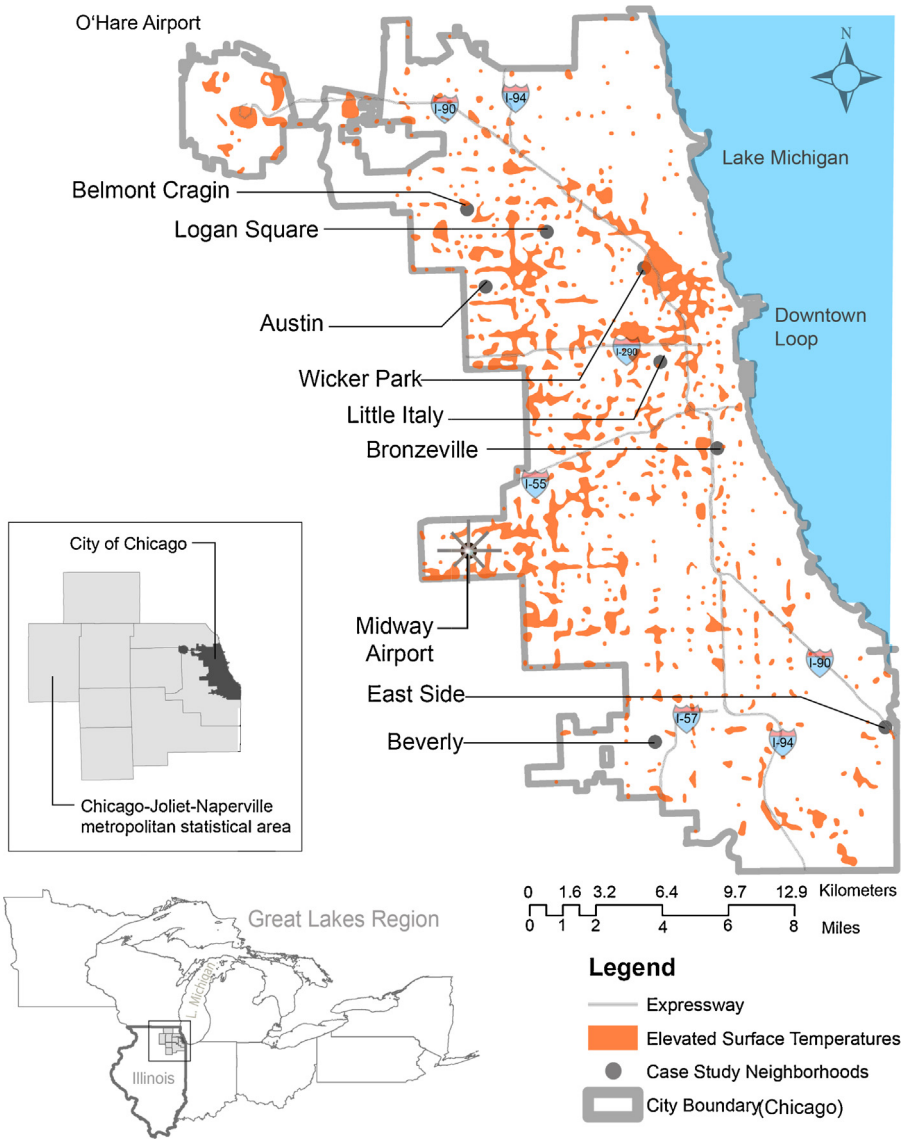

Fig. 1. Map of the Eight Study Neighborhoods. The eight county Chicago–Joliet–Naperville metropolitan statistical area lies on west side of Lake Michigan within the Great Lakes region (context maps not to scale). The large map illustrates the City of Chicago municipal boundaries, the location of the eight study neighborhoods, Midway Airport, and the heterogeneous distribution of elevated surface temperatures from a City of Chicago Department of the Environment 2006 study.

Data sources: City of Chicago map – from the City of Chicago Department of Environment GIS database, accessed February 1, 2010. Chicago–Joliet–Naperville metropolitan statistical area map – from the U.S. Department of Commerce, U.S. Census Bureau, Geography Division, 2010 Census Metropolitan Statistical Area/Micropolitan Statistical Area (CBSA), accessed February 9, 2014 from http://crystal.isgs.uiuc.edu/nsdihome/. Great Lakes region map – from the from the North American Transportation Atlas Data – 1998, prepared by the U.S. Department of Transportation, Bureau of Transportation Statistics, accessed February 9, 2014 from http://www.glin.net/gis/data/refdata.html. Illustration by authors.

Table 1
Neighborhood characteristics in 2010 US census.

	E–W street orientation				N–S street orientation			
	Wicker Park	Little Italy	Austin	Beverly	Logan Square	Bronzeville	Belmont Cragin	East Side
2010 median household income	$84,205	$42,663	$31,263	$56,346	$43,116	$19,316	$40,528	$38,032
% Non-White	21.7%	33.5%	96.8%	66.3%	48.8%	88.9%	44.9%	46.3%
Density of dwelling units/ha (/acre)[a]	47.4 (19.2)	30.9 (12.5)	35.3 (14.3)	14.3 (5.8)	27 (10.9)	35.7 (14.4)	26 (10.5)	19.2 (7.8)
Density of people/ha (/acre)[a]	94.8 (38.4)	55.1 (22.3)	92 (37.2)	30 (12.1)	70.6 (28.6)	58.9 (23.8)	83.5 (33.8)	56.8 (23)

Note: City of Chicago 2010 statistics below from the 2010 U.S. Census accessed June 10, 2013. 2010 Median household income in Chicago was $46,877 ± 400. 2010% Non-White in Chicago was 55%. 2010% African-American of total non-white in Chicago was 59.9%. 2010 population density in Chicago was 45.7 persons per ha.

[a] Using USGS orthoimagery image from April 2010, site visits, and a mailbox inventory.

Table 2
Land use/land cover, building configuration, and adjacent heat sources and sinks variables for the eight neighborhoods in 2010.

	E–W street orientation				N–S street orientation			
	Wicker Park	Little Italy	Austin	Beverly	Logan Square	Bronzeville	Belmont Cragin	East
Land cover								
% impervious[*,d]	95.7	94.3	75.1	54.6	88.1	79.9	78	73.5
% roof cover[d]	34	39.1	28.2	22.9	37.9	21.8	37.9	31.9
% tree canopy[d]	4.7	29.4	19.7	60.4	13.2	18.5	18.1	23.1
Building configuration								
Urban canyon ratio[b]	0.78	0.6	0.31	0.24	0.44	0.28	0.32	0.29
Avg building height (m)[b]	13.8	13	10.8	9.1	12.4	9.1	10.4	9.9
Sky view factor[c]	0.53	0.49	0.7	0.51	0.66	0.65	0.67	0.69
Alley orientation[b]	E–W	E–W	E–W	E–W	N–S	N–S	N–S	N–S
Adjacent heat sources/sinks								
% upwind tree canopy[d]	11	30	23.3	49.5	8.3	14	12.7	18.1
Avg upwind building height (m)[b]	14.3	15.2	10.7	9.1	12.2	10.7	10.4	9.8
Distance to lake (km)[a]	3.6	3.7	11.4	11.5	8	1.4	11.6	0.4
Distance to downtown (km)[a]	3.3	2.1	10.5	19.2	8.3	4.6	12.4	20.3
Distance to nearby upwind industrial (km)[a]	2.6	1.7	2.1	5.9	0.2	1.6	1.4	1.9
Distance to nearby upwind freeway (km)[a]	4.8	7.3	4.5	7.5	8.1	1.1	9	7.1
Distance to nearby upwind park (km)[a]	4.4	9.2	6.5	2.7	11.5	9.1	1	1.5
*% of total impervious that was roof	35.6%	41.5%	37.6%	41.8%	43.1%	27.3%	48.6%	43.3%

[*] % of total impervious that was roof.
[a] Calculated using Google Earth.
[b] Calculated using site visits and Chicago Zoning Code Summary of standard building heights.
[c] Calculated using Solmetric SunEye.
[d] Calculated using USGS orthoimagery image from April 2010.

We quantified 14 physical characteristics (independent variables) of each block for this study. We created three land use/land cover variables: (1) percent impervious surface (roofs and pavements only), (2) percent roof (included in impervious surface), and (3) percent tree canopy. For each neighborhood's land cover variables, we used USGS high-resolution orthoimagery from April 9, 2010 to calculate the areas and determine the relative percentages of each block. It is important to note that to increase the precision of our measurements, we accounted for the impervious surfaces beneath the tree canopy in a method similar to Akbari, Rose, and Taha (2003). Impervious surface measurements that do not account for the area beneath tree canopies miss a large percentage of impervious surfaces in urban areas with large tree canopies.

For each neighborhood's building configuration, we created four independent variables to represent important characteristics derived from the literature review. These were (1) average building height by block, (2) alley urban canyon ratio, (3) SVF at the HOBO, and (4) alley orientation. For the urban canyon ratio and the building heights, we calculated these using aerial orthoimagery, site visits, and the Chicago Zoning Code Summary of standard building heights for each neighborhood's building type (Chicago Zoning Code, 2012). We calculated the sky view factors (SVF) below each weather station in a manner similar to Svensson (2004) using a Solmetric SunEye. Orientation of the urban canyon was calculated as a dummy variable, either 0 for north–south oriented alleys or 1 for east–west oriented alleys.

For each neighborhood's adjacent heat sources and sinks, we calculated seven variables. Based on Oke's research (2004), we created an elliptical shape that measured 0.50 km by 0.33 km with the long axis oriented upwind from the neighborhood. From this elliptical area, we quantified the average upwind building height and percent upwind tree canopy. Then we measured the shortest distances from each HOBO weather station to (1) Lake Michigan, (2) the downtown core, (3) nearest upwind industry, (4) nearest upwind freeway, and (5) nearest upwind park.

While the neighborhoods vary in their physical characteristics, an interesting pairing emerges. Both Wicker Park and Little Italy are largely impervious; 95.7% and 94.3% respectively. However, the amount of tree canopy varies significantly, from 4.7% in Wicker Park to 29.4% in Little Italy. Many of the additional physical measurements are relatively comparable and both have an east–west street orientation. Therefore, this pairing of Wicker Park and Little Italy should yield some interesting results. Also by reviewing these descriptive characteristics, we confirm our observation that Beverly has a smaller percentage of impervious surface (54.6%) and the highest percentage of tree canopy (60.4%) relative to the other neighborhoods.

2.4. Controlling for weather: clear skies and heat events

UHI patterns and intensity change under different weather conditions (Klysik & Fortuniak, 1999; Stewart, 2011). We controlled for weather to (1) isolate the urban-induced warming and (2) identify the most dangerously hot days. To isolate urban-induced warming, we selected only days with clear skies (24 h of clear skies) as recommended by Stewart (2011). This reduced the number of days we analyzed from 62 days to 12 clear days. Next, due to the dangers of heat, Sheridan (2012) has developed a system to classify days when extreme heat has raised the risk of heat related illness. Sheridan's (2012) *Spatial Synoptic Classification System* classifies days when extreme heat or the combination of heat and humidity raise the risks of heat related illness. The National Weather Service's heat warning system considers the two variables of air temperature and humidity. Sheridan's (2012) system classifies days as dangerous based on four daily readings of air temperature, dew point, wind, pressure, and cloud cover. We used Sheridan's classifications to identify extreme heat event days from the 12 clear days. Only two of the 12 clear days were classified as heat event days.

3. Results

Although not an extreme summer in terms of the number of heat events, the summer of 2010 was consistently warm. To begin, we explored the effect of controlling for heat event days only, clear skies only, and the combination of heat event days with clear skies to understand how this affected UHI intensity (see Appendix B for the complete temperature record). Figs. 2 and 3 show nighttime (2 a.m.) and daytime (4 p.m.) UHI intensity (C) in the eight neighborhoods relative to Midway Airport during 12 clear days and two heat event days. For the 12 clear days, the warmest

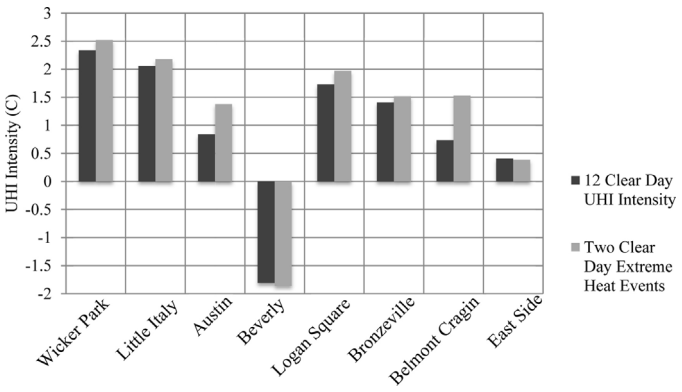

Fig. 2. Nighttime (2 a.m.) air temperature differences.

neighborhood at 2 a.m. was Wicker Park averaging +2.34 °C (±0.73) and the coolest neighborhood was Beverly with average air temperatures −1.81 °C (±0.85). At 4 p.m., Belmont Cragin was the warmest neighborhood with average readings +2.68 °C (±0.59) and Beverly remained the coolest neighborhood. Using ANOVA, we found that there was a statistically significant difference between the eight neighborhoods' air temperatures at both 2 a.m. ($F = 28.91$, df = 7.88) and 4 p.m. ($F = 6.04$, df = 7.88) at the 0.001 level.

3.1. Bivariate correlations

First, we conducted a bivariate analysis (Table 3) to understand the relationship between each neighborhood's UHI intensity at 2 a.m. and 4 p.m. and the 14 independent variables. At 2 a.m., the 11 significant bivariate correlations ($p = .01$) were (1) percent impervious surface (.82), (2) percent tree canopy (−.72), (3) distance to downtown (−.70), (4) average upwind building heights (.67), (5) distance to nearby upwind industrial (−.65), (6) average building heights (.63), (7) percent upwind tree canopy (−.62), (8) urban canyon ratio (.60), (9) percent of roof (.47), (10) distance to nearby upwind park (.46), and (11) distance to lake (−.40). At 4 p.m., the seven significant bivariate correlations ($p = .01$) were (1) distance to nearby upwind industrial (−.52), (2) percent upwind tree canopy (−.48), (3) percent tree canopy (−.44), (4) SVF (.38), (5) street orientation (−.36), (6) percent roof area (.33), and (7) percent impervious (.30). This bivariate analysis is an interesting opportunity to understand the discrete relationships between the dependent and independent variables before we combine these in more complex methods. In general, the strength of the bivariate relationships between the independent variables and UHI intensity was greater at 2 a.m. than at 4 p.m.

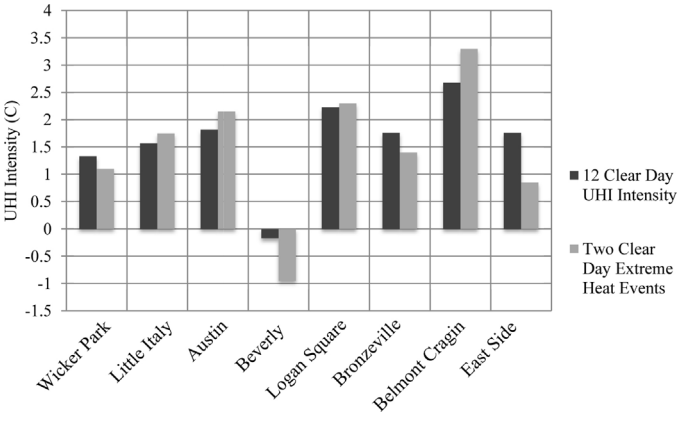

Fig. 3. Daytime (4 p.m.) air temperature differences.

Table 3
Bivariate correlations between physical characteristics and the UHI intensity at 2 a.m. and 4 p.m.

	UHI intensity		Land cover			Neighborhood configuration				Adjacent heat sources and sinks					
	2 a.m.	4 p.m.	% ISA[c]	% roof	% tree canopy	UC[d] ratio	Build ht. of block	SVF	Orien. (0, 1)	% upwind tree canopy	Ave upwind build ht.	Dist. to lake	Dist. to down-town	Dist. to nearby indust.	Dist. to nearby fwys.	Dist. to nearby parks
Neighborhood	−.23[a]	−.10	−.19	.20[a]	.08	.01	.11	.07	−.18	−.03	−.21[a]	.09	.55[b]	.11	.55[b]	−.22[a]
UHI intensity 2 a.m.		.19	.82[b]	.47[b]	−.72[b]	.60[b]	.63[b]	.03	−.07	−.62[b]	.67[b]	−.40[b]	−.70[b]	−.65[b]	−.22[a]	.46[b]
UHI intensity 4 p.m.			.30[b]	.33[b]	−.44[b]	.03	.12	.38[b]	−.36[b]	−.48[b]	.08	−.04	−.17	−.52[b]	.04	.10
% impervious				.67[b]	−.78[b]	.83[b]	.85[b]	−.14	.00	−.66[b]	.89[b]	−.45[b]	−.84[b]	−.70[b]	−.12	.51[b]
% roof					−.46[b]	.55[b]	.72[b]	−.05	−.10	−.43[b]	.60[b]	.01	−.30[b]	−.59[b]	.64[b]	.10
% tree canopy						−.49[b]	−.53[b]	−.43[b]	.33[b]	.95[b]	−.44[b]	.35[b]	.55[b]	.81[b]	.27[b]	−.26[a]
Urban canyon							.94[b]	−.55[b]	.42[b]	−.30[b]	.92[b]	−.31[b]	−.70[b]	−.21[a]	−.00	.24[a]
Building ht. of block								−.39[b]	.37[b]	−.36[b]	.91[b]	−.15	−.66[b]	−.38[b]	.17	.37[b]
SVF									−.68[b]	−.55[b]	−.54[b]	.07	.30[b]	−.54[b]	−.12	−.05
Orientation										.60[b]	.39[b]	.25[a]	−.20[a]	.57[b]	−.06	−.01
% upwind tree canopy											−.25[a]	.34[b]	.41[b]	.86[b]	.19	−.23[a]
Ave upwind build ht.												−.34[b]	−.83[b]	−.36[b]	−.02	.49[b]
Distance to lake													.28[b]	.30[b]	.44[b]	−.19
Distance to downtown														.47[b]	.42[b]	−.67[b]
Distance to nearby upwind industrial															.04	−.49[b]
Distance to nearby upwind freeway																−.32[b]

[a] Correlation is significant at the 0.05 level (2-tailed).
[b] Correlation is significant at the 0.01 level (2-tailed).
[c] Impervious surface area.
[d] Urban canyon.

3.2. Regression analysis

Next we preformed an ordinary least squared (OLS) regression analysis to determine the explanatory power of independent variables for the 2 a.m. UHI intensity. We entered our variables in blocks. Model One included the neighborhood identifier. In Model Two we added the percentage of impervious and the percentage of tree canopy of the block. In Model Three, we added the independent variables urban canyon ratio and orientation.

Examining the regression analysis using the 12 clear days only, at 2 a.m. ($n = 96$), Model Three explains 68% of the variance in the UHI intensity (Table 4). Overall this model is significant with an *F*-value of 40.62. The only significant predictor in Model Three at 2 a.m. was percent impervious of the block ($p < 0.001$ level). All other independent variables were not significant predictors of the UHI intensity at 2 a.m. Neighborhoods with more impervious surfaces were warmer. Controlling for all other factors, a neighborhood's air temperature warmed by +0.97 °C at 2 a.m. for every additional 10% increase in impervious surfaces area of the block. In comparison to the land cover factors, neighborhood building configuration variables were not significant at 2 a.m. Interestingly, Model Two had two significant factors, percent impervious ($p < 0.001$ level) and percent tree canopy ($p < 0.05$ level). Without controlling for neighborhood building configuration, tree canopy is a significant predictor of neighborhood UHI intensity.

Rerunning the regression model at 2 a.m. ($n = 16$) during heat events, Model Three improved in its explanatory power. It explained 90% of the variance in UHI intensity (Table 5). Overall the Model Three is significant with an *F*-value of 27.18. The significant predictors of UHI intensity during heat event days were the percentage of impervious surface ($p < 0.005$ level) and percent tree canopy ($p < 01$ level). During heat event days and controlling for all other variables, for every 10% increase in impervious surfaces of the block we would expect a warming of +0.93 °C. Controlling for all other variables during heat event days, for every 10% increase in tree canopy of the block we would expect a cooling of −0.33 °C relative to Midway.

In the 4 p.m. model, we substituted adjacent heat sources and sink variables for building configuration variables. Again we entered our variables in blocks. Models One and Two were identical to the 2 a.m. regression including the variables for neighborhood identifier and land use/land cover variables for percent impervious surface and percent tree canopy. At 4 p.m., Model Three included variables for distance to nearest upwind industrial location and percent tree canopy in the adjacent upwind area.

At 4 p.m. during the 12 clear days ($n = 96$), Model Three explains 26% of the variance in the UHI intensity and has one significant predictor (Table 6). Model Three explanatory power is significantly improved over Model Two for 4 p.m. Overall, Model Three is significant with an *F*-value of 7.50. In Model Three, for every additional 1.0 km increase in distance from industrial areas we would expect a neighborhood to be −0.45 °C cooler ($p < 0.05$ level). The analysis suggests that predicting daytime UHI intensity is more difficult than predicting nighttime UHI intensity. In addition, higher wind speeds during the day likely displace elevated air temperatures from upwind locations, such as industrial sites.

Running the regression model for two clear heat event days at 4 p.m. ($n = 16$), Model Three explained only 12% of the variance in UHI intensity (Table 7). Overall the model is not significant with an *F*-value of 1.39. All predictors of UHI intensity are insignificant during heat events in the late afternoon (4 p.m.). This further illustrates the lower ability to explain the UHI intensity in the afternoon, especially during heat events. Yet, caution should be exercised when interpreting these results due to the limited number of heat event days in the data set.

Finally, in our small sample of eight neighborhoods, we found that income was not correlated with higher summertime temperatures. Our results show that the warmest neighborhoods during the 12 clear days (Wicker Park at 2 a.m. and Belmont Cragin at 4 p.m.) were not the poorest neighborhoods. In this small sample of eight neighborhoods there was no correlation between elevated air temperature, median household income, or percentage of tree canopy. The lowest income neighborhood (Bronzeville with a median household income in 2010 of $19,316) had 18.5% tree canopy. Whereas higher income neighborhoods such as Wicker Park and Logan Square with median household incomes in 2010 of $84,205 and $43,116 (Table 1) respectively had lower percentages of tree canopy (Wicker Park 4.7% and Logan Square 13.2% tree canopy). In addition, both Wicker Park and Logan Square were consistently warmer than Bronzeville at 2 a.m. and 4 p.m. However, the small sample size limits our confidence in this finding.

4. Discussion

The physical characteristics that explained the greatest proportion of the neighborhood's nighttime temperature difference were the percentages of impervious surface and tree canopy. These two factors explained 68% of the variance in air temperature at 2 a.m. Contrary to our hypothesis that adding the local building characteristics would enhance the explanatory power of the model, the addition of urban canyon ratio and the street orientation had no significant impact on our ability to explain air temperature. From the 2 a.m. regression analysis, we learn for every 10% of additional impervious surface area we would expect an increase of 0.74 °C and for every 10% of additional tree canopy, we would expect a temperature decrease of 0.2 °C. During the two heat events, these two land use/land cover variables increased to explain 91% of each urban block's air temperature. During the two heat extremes, the importance of tree canopy increased slightly and the importance of impervious surface declined slighted. Therefore, during a heat event, for every 10% of additional impervious surface area, we would expect an increase of 0.62 °C and for every 10% of additional tree canopy, we would expect a temperature decrease of 0.35 °C.

Fig. 2 (Nighttime Temperature Differences) illustrates these findings. In this figure, the four E–W neighborhood blocks are grouped on the left and the four N–S neighborhoods are grouped on the right. Within the two groups, the neighborhood blocks with the highest percentage of impervious surface are on the left and decrease in percentage toward the right. With the exception of the East Side block, the UHI intensity decreases with the amount of impervious surface and the UHI intensity was greater during the heat events relative to the other days. The Beverly block was notably cooler than the Midway station and at 2 a.m. this difference between the warmest block in Wicker Park and the coolest block in Beverly was approximately 4 °C. This is approximately 2 °C less than Imhoff and colleagues (2010) estimated the UHI effect for a city in a temperate grassland bioclimatic region.

Another striking feature of this graph is the opportunity to 'see' how vegetation influenced nighttime air temperature and ground-truth the findings of our regression analysis. The Wicker Park block was 95.7% impervious and had only 4.7% covered with tree canopy. The Little Italy block was 94.3% impervious but had 29.4% or 6 times the percentage of tree canopy. At 2 a.m. in average summer conditions, the difference in the UHI intensity between Wicker Park and Little Italy was +0.27 °C (Wicker Park warmer) and during heat events this increased to +0.35 °C. This is a nice example of how the addition of vegetation in extremely dense urban areas

Table 4
Regression analysis for UHI temperatures at 2 a.m. in eight Chicago neighborhoods during 12 clear days in summer 2010.

Variable	Model 1			Model 2			Model 3		
	B	SE	Beta	*B*	SE	Beta	*B*	SE	Beta
Neighborhood	−.12*	.05	−.23	−.05	.03	−.09	−.02	.04	−.04
% impervious				7.42***	1.12	.63	9.66***	2.58	.82
% tree canopy				−2.07*	.88	−.22	−1.79	1.04	−.19
Urban canyon							−1.58	1.74	−.19
Orientation							.18	.35	.06
(Constant)	1.58***	.31		−4.23***	1.11		−5.67***	1.84	
n		96			96			96	
Adjusted R^2			.04			.68***			.68
Change in R^2						.64			.00

* $p < .05$.
** $p < .01$.
*** $p < .005$ (one-tailed tests).

Table 5
Regression analysis for UHI temperatures at 2 a.m. during heat events in eight Chicago neighborhoods during two clear days in summer 2010.

Variable	Model 1			Model 2			Model 3		
	B	SE	Beta	*B*	SE	Beta	*B*	SE	Beta
Neighborhood	−.15	.12	−.31	−.08	.04	−.16	−.04	.06	−.08
% impervious				6.21***	1.40	.58	9.27*	3.34	.86
% tree canopy				−3.47**	1.10	−.40	−3.29*	1.35	−.38
Urban canyon							−2.30	2.26	−.31
Orientation							.35	.45	.13
(Constant)	1.95*	.71		−2.55	1.39		−4.46	2.39	
n		16			16			16	
Adjusted R^2			.03			.91***			.90
Change in R^2						.83			.00

* $p < .05$.
** $p < .01$.
*** $p < .005$ (one-tailed tests).

Table 6
Regression analysis for UHI temperatures at 4 p.m. in eight Chicago neighborhoods during 12 clear days in summer 2010.

Variable	Model 1			Model 2			Model 3		
	B	SE	Beta	*B*	SE	Beta	*B*	SE	Beta
Neighborhood	−.05	.05	−.10	−.04	.05	−.08	−.04	0.05	−.07
% impervious				−1.38	1.68	−.13	−2.20	1.97	−.20
% tree canopy				−4.65***	1.32	−.53	−.86	3.75	−.10
Distance to industry							−.45*	.18	−.51
% upwind tree canopy							−.01	.05	−.08
(Constant)	1.86***	.29		4.00*	1.66		4.92**	1.83	
n		96			96			96	
Adjusted R^2			−.00			.17***			.26***
Change in R^2						.19			.09

* $p < .05$.
** $p < .01$.
*** $p < .005$ (one-tailed tests).

Table 7
Regression analysis for UHI temperatures at 4 p.m. during heat events in eight Chicago neighborhoods during two clear days in summer 2010.

Variable	Model 1			Model 2			Model 3		
	B	SE	Beta	*B*	SE	Beta	*B*	SE	Beta
Neighborhood	−.13	.15	−.21	−.11	0.15	−.18	−.09	.16	−.15
% impervious				−.68	5.11	−.05	−2.66	6.31	−.21
% tree canopy				−5.52	4.02	−.54	−3.29	12.02	−.32
Distance to industry							−.68	.58	−.66
% upwind tree canopy							.03	.15	.21
(Constant)	2.11*	.87		3.85	5.06		5.76	5.87	
n		16			16			16	
Adjusted R^2			−.02			.11			.12
Change in R^2						.24			.12

* $p < .05$.
** $p < .01$.
*** $p < .005$ (one-tailed tests).

can reduce air temperatures and again reminds us that the presence of impervious surface is not synonymous with the absence of vegetation.

Relative to the 2 a.m. time, the significant characteristics that explained air temperature at 4 p.m. varied. When we included only the percentage of impervious and percentage of tree canopy, the greatest proportion of a neighborhood's UHI intensity was explained by a neighborhood's percentage of tree canopy. However, tree canopy only explained 17% of the variation in afternoon air temperature. We hypothesized that in the afternoon when winds were higher, the adjacent heat sources and sinks would be more important than the local building configuration. When we added distance to industry and percentage upwind tree canopy, the distance to industry became the only significant explanatory variable and the model's explanatory powered increased slightly. From the regression analysis, we learn for every 1.0 km farther from an industrial site, the block temperature was 0.45 °C cooler. Interestingly, while the predictors of the 2 a.m. temperature increased in their predictive power during extreme heat, none of the independent variables significantly explained the UHI intensity at 4 p.m. during heat events.

To contextualize this finding, we can return to the Wicker Park and Little Italy comparison. At 4 p.m., the average air temperature during the 12 clear days in Little Italy was 30.9 °C and the temperature in Wicker Park was 30.7 °C. The Little Italy block is about 1 km closer (1.7 km) to an upwind industrial site than the Wicker Park block (2.6 km). In average summer conditions at 4 p.m. the change in UHI between Wicker Park and Little Italy was −0.24 °C (Wicker Park cooler) and during heat events this decreases to −0.65 °C. In late afternoon, waste heat from industrial areas increased temperatures in the neighborhood despite the increased tree canopy.

5. Conclusion

This research makes several contributions to the literature. One contribution is our selection of variables from both the remote sensing literature and the urban climatology literature to explain air temperature variation at the urban block level. By investigating the effect of fourteen variables on air temperature we were able to assemble a subset of simple measurements to understand UHI variation at the urban block scale for different times of day. In future research, we would like to compare our findings with Stewart and Oke's (2012) more detailed approach using Local Climate Zones to evaluate whether their typologies add accuracy in estimating UHI air temperatures.

Another contribution is our finding that using daily mean air temperatures to examine UHIs may mask important differences between the physical mechanisms contributing to high daytime and nighttime air temperatures. We found that land cover variables significantly contributed to nighttime UHIs but during the day the most significant contributors to UHIs were upwind conditions. At nighttime, the percentage of impervious surface and tree canopy within an urban block explained 68% of the air temperature. The strength of this relationship increased during heat events and these two variables explained 91% of variation in block air temperature. Interestingly, our finding that every 10% increase in impervious surface, increased nighttime air temperature by 0.74 °C is very close to Klock and colleagues' (2012) finding. They found that for every 10% increase in impervious surface, the surface temperature of the city district increased by 0.7 °C. In our study, during non-heat extremes, for every 10% increase in the percentage of tree canopy explained a 0.2 °C decrease in air temperature variation while Klock and colleagues (2012) found that the percentage of green space within the district explained a 1.3 °C decrease.

From a public health perspective, minimizing nighttime air temperatures in residential neighborhoods is critical to minimize sleep disturbances. First, any unnecessary impervious surfaces on the ground plain should be removed and replaced with vegetation (if possible). Roof areas also contribute to amount of impervious surface. Cool roofs can refer to techniques that apply reflective coatings or increasing the presence of green roofs. Reflective roof coatings would increase the amount of reflected solar radiation and green roofs would lower temperatures and add moisture. Our research also supports the importance of vegetation on the ground plane, particularly trees on east–west streets that would increase daytime shading as well as add moisture. New research is questioning whether reflective pavements and porous pavements actually decrease air temperature in denser urban areas but more research is needed to confirm this (Stempihar, Pourshams-Manzouri, Kaloush, & Rodezno, 2012, Self-citation).

Another important contribution of our research is the identification of the importance of waste heat to daytime UHIs. Stone (2012) identified four principle characteristics that make cities hotter than surrounding areas. These characteristics were (1) the reduction in evaporative cooling, (2) low surface reflectivity, (3) vertical surfaces, and (4) waste heat. Much of the literature has focused on the first three principles and the subject of waste heat has received less attention. Moving forward, we need to consider including waste heat sources and improve our measurement of their contribution to elevated air temperatures. We may wish to identify waste heat priority zones in locations where the ratio of waste heat emitted from industrial processes, vehicular traffic, or air conditioning, exceeds surface-emitted heat. One weakness of our study is how we simplistically measured waste heat by using the distance to industrial sites and we assumed the amount of waste heat generated within the largely residential neighborhoods would be relatively comparable. We did not consider the type of industry or the characteristics of the industrial site (most of these site have large impervious areas with little tree canopy). From an urban planning perspective, we need to be thinking more about waste heat sources, wind patterns, and the strategic placement of vegetative buffers.

Acknowledgments

We would like to thank the Graham Environmental Sustainability Institute for their financial support of this research and to Dr. Marie O'Neill for the use of her HOBO weather stations. We would also like to thank the Chicago Department of Transportation for the logistical support that made the study possible.

Appendix A. Selection of midway airport weather station relative to other area weather stations (includes a figure, uploaded separately)

Midway appendix

Data from Midway Airport was used to calculate baseline air temperature, relative humidity, wind speed and direction, and sky condition. Past UHI studies in the Chicago region have used O'Hare (McPherson et al., 1997) while other more recent studies have used multiple urban and suburban sites within the Chicago region (Gray & Finster, 2000). For this study we used Midway Airport and not O'Hare Airport because the predominate wind direction during the study period was out of the southwest direction (210°), so Midway (due to its more southwesterly location) provides a better comparison before air

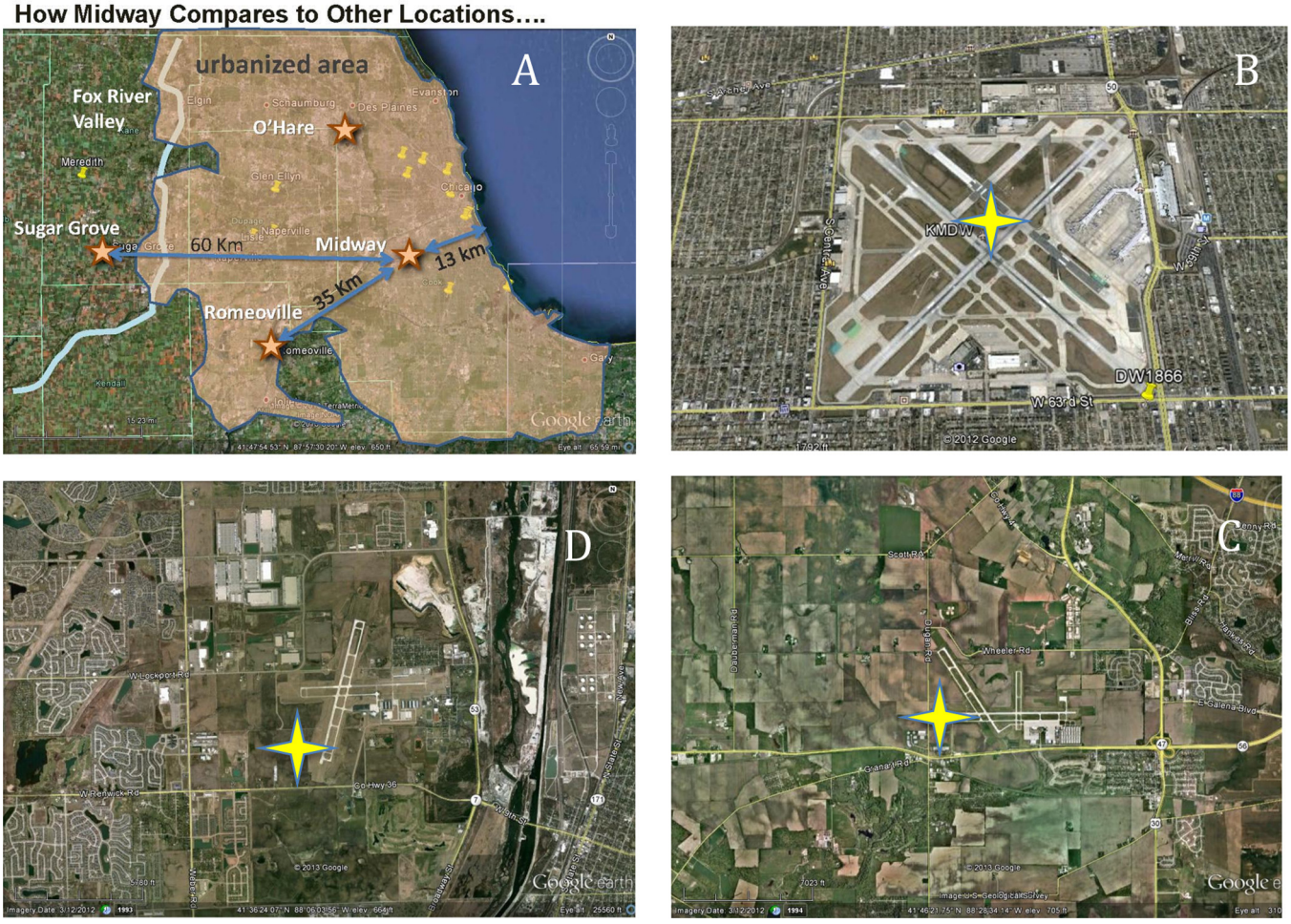

Fig. A1. Explanation of Midway Airport as the Base Location. Urbanized land use/land cover spreads as far as 70 km west of Lake Michigan (A). The three airport's land covers and weather station locations (yellow star) are shown above (B–D). Midway Airport* (B) relative to other regional weather stations located at Romeoville** (KLOT) (D) and Sugar Grove *** (KARR) (C), not to scale. *Location of Midway Airport (KMDW) weather station (indicated by star) as documented by http://weather.gladstonefamily.net/site/KMDW, accessed December 30, 2012, not to scale. *Photograph: Google Earth*. **Location of Romeoville (KLOT) weather station (indicated by star) as documented by http://weather.gladstonefamily.net/site/KLOT, accessed December 30, 2012, not to scale. *Photograph: Google Earth*. *** Location of Sugar Grove (KARR) weather station (indicated by star) as documented by http://weather.gladstonefamily.net/site/KARR, accessed December 30, 2012, not to scale. *Photograph: Google Earth*.

masses move over the urban neighborhoods. Although Midway is well within the Chicago urbanized region the airport's open character allows for ventilation and mixing of the air. In addition, the weather station is located at the center of the tarmac (image B) west of the terminal building, and away from idling jets. Finally, although impervious surfaces cover roughly 61% of the airport grounds, as calculated from aerial orthoimages, the runways are lighter colored concrete that should absorb less solar radiation than asphalt.

We considered using two other weather stations to measure base weather conditions, a suburban station in Romeoville, IL (image C) and a rural station in Sugar Grove, IL (image D). First, Romeoville was surrounded by low-density suburban development and at least 45 km southwest of Chicago's downtown Loop (image A). In addition, the Romeoville site was missing some data from a few critical clear days.

Although Sugar Grove was the closest rural weather station west of the neighborhoods it was approximately 70 km from the downtown Loop area (image A). Sugar Grove (image D) was not used because of the large distance from the urban core and Lake Michigan. In addition, the Fox River Valley results in topographical changes between Sugar Grove and the eight neighborhoods, which may have influenced air temperatures (Fig. A1).

Appendix B. Exploration of controlling for weather conditions

To begin, we explored the effect of controlling for heat event days, clear skies, and heat event days with clear skies to understand how this affected UHI intensity. The table below describes four different types of UHI intensity analysis between the neighborhoods and Midway Airport during July and August 2010 using data from (1) all 62 days, (2) 12 heat event days with or without cloud cover only, (3) 12 clear days only, and (4) two clear heat event days only. First, to select the 12 heat event days (clear and cloudy) we used Sheridan's (2012) Spatial Synoptic Classification System to identify days when the combination of heat and humidity pose a dangerous threat to residents. Then, to isolate urban factors that contributed to the warming (UHI) in the eight neighborhoods, we selected only days with clear skies with light winds (24 h of clear skies and relatively light winds) as recommended by urban climate researchers (Bonacquisti et al., 2006; Gedzelman et al., 2003; Kim & Baik, 2002; Klysik & Fortuniak, 1999; McPherson et al., 1997; Stewart, 2011). This reduced the number of days we analyzed from 62 days to 12 clear days. Finally, of the 12 clear days we selected the only two clear heat event days, to again isolate the urban-induced warming during heat waves.

Air temperature difference from midway airport during July and August 2010.

Neighborhood	All days (n = 62) temperature differences		12 heat event days[a] (n = 12)		12 clear days[b] UHI (n = 12)		2 heat events with clear skies[c] UHI (n = 2)	
	C	F	C	F	C	F	C	F
2 a.m.								
Wicker Park	1.93	3.47	1.59	2.86	2.34	4.21	2.52	4.54
Little Italy	1.67	3.00	1.29	2.33	2.06	3.71	2.18	3.92
Austin	0.83	1.49	0.93	1.67	0.84	1.51	1.38	2.48
Beverly	−1.04	−1.88	−0.86	−1.54	−1.81	−3.26	−1.86	−3.34
Logan Square	1.41	2.54	1.28	2.31	1.73	3.12	1.97	3.55
Bronzeville	0.99	1.78	0.56	1.01	1.41	2.54	1.52	2.73
Belmont Cragin	0.75	1.34	0.91	1.64	0.74	1.34	1.53	2.75
East Side	0.35	0.62	−0.06	−0.11	0.41	0.74	0.39	0.70
Total	0.86	1.55	0.71	1.27	0.97	1.74	1.20	2.16
4 p.m.								
Wicker Park	1.00	1.81	1.27	2.28	1.33	2.39	1.10	1.98
Little Italy	1.01	1.83	1.27	2.28	1.57	2.82	1.75	3.15
Austin	1.59	2.86	1.51	2.72	1.82	3.27	2.15	3.87
Beverly	−0.06	−0.12	−0.68	−1.22	−0.17	−0.3	−0.95	−1.71
Logan Square	2.00	3.60	1.93	3.48	2.23	4.01	2.30	4.14
Bronzeville	0.90	1.61	1.12	2.01	1.76	3.17	1.40	2.52
Belmont Cragin	2.22	3.99	2.27	4.08	2.68	4.83	3.30	5.94
East Side	0.94	1.69	1.28	2.3	1.76	3.17	0.85	1.53
Total	1.20	2.16	1.24	2.24	1.62	2.92	1.49	2.68

[a] Heat Event days as derived from Sheridan's (2012) Spatial Synoptic Classification system calculated at O'Hare Airport.

[b] Clear days are days with 24 hourly Midway Airport sky conditions reported as clear, mostly clear, or partly cloudy.

[c] Heat event days with clear skies only derived from Midway Airport sky condition observations and Sheridan's (2012) Spatial Synoptic Classification system calculated at O'Hare Airport.

Positive numbers indicate warmer conditions in degrees (C = Celsius, F = Fahrenheit).

References

Akbari, H., Rose, L. S., & Taha, H. (2003). Analyzing the land cover of an urban environment using high-resolution orthophotos. *Landscape and Urban Planning*, *63*, 1–14.

Ali-Toudert, F., & Mayer, H. (2007). Effects of asymmetry, galleries, overhanging facades and vegetation on thermal comfort in urban street canyons. *Solar Energy*,

Angel, J. (2013). *Climate of Chicago – Description and normals*. Retrieved from: http://www.isws.illinois.edu/atmos/statecli/general/chicago-climate-narrative.htm

Ackerman, B. (1985). Temporal march of the Chicago heat island. *Journal of Climate and Applied Meteorology*, *24*, 547–554.

Bonacquisti, V., Casale, G. R., Palmieri, S., & Siani, A. M. (2006). A canopy layer model and its application to Rome. *Science of the Total Environment*, *364*, 1–13.

Britter, R. E., & Hanna, S. R. (2003). Flow and dispersion in urban areas. *Annual Review of Fluid Mechanics*, *35*, 469–496.

Chang, C., Li, M., & Chang, S. (2007). A preliminary study on the local cool-island intensity of Taipei City parks. *Landscape and Urban Planning*, *80*, 386–395.

Chicago Zoning Code. (2012). *Chicago zoning code summary*. Retrieved from: http://www.clvn.org/pdf/zoningCodeSummary.pdf

City of Chicago. (2006). *Elevated surface temperature map*. City of Chicago Dept. of Planning and Development.

Djen, C. S., Jingchun, Z., & Lin, W. (1994). Solar radiation and surface temperature in Shanghai City and their relation to urban heat island intensity. *Atmospheric Environment*, *28*(12), 2119–2127.

Eliasson, I. (1996). Urban nocturnal temperatures, street geometry, and land use. *Atmospheric Environment*, *30*(3), 379–392.

Fan, H., & Sailor, D. J. (2005). Modeling the impacts of anthropogenic heating on the urban climate of Philadelphia: A comparison of implementations in two PBL schemes. *Atmospheric Environment*, *39*, 73–84.

Gedzelman, S. D., Austin, S., Cermak, R., Stefano, N., Partridge, S., Quesenberry, S., et al. (2003). Mesoscale aspects of the urban heat island around New York City. *Theory of Applied Climatology*, *75*, 29–42.

Gray K. and Finster M., 2000. The urban heat island, photochemical smog, and Chicago: Local features of the problem and solution, Atmospheric Pollution Prevention Division U.S. Environmental Protection Agency, Retrieved from http://www.epa.gov/heatisland/resources/pdf/the_urban_heat_island.pdf

Hayhoe, K., Sheridan, S., Kalkstein, L., & Greene, S. (2010). Climate change, heat waves, and mortality projections for Chicago. *Journal of Great Lakes Research*, *36*, 65–73.

Imhoff, M. L., Zhang, P., Wolfe, R. E., & Bounoua, L. (2010). Remote sensing of the urban heat island effect across biomes in the continental USA. *Remote Sensing of Environment*, *114*, 504–513.

Jenerette, D. G., Harlan, S. L., Brazel, A., Jones, N., Larsen, L., & Stefanov, W. L. (2007). Regional relationships between surface temperature, vegetation, and human settlement in a rapidly urbanizing ecosystem. *Landscape Ecology*, *22*(3).

Johnson, G. T., Oke, T. R., Lyons, T. J., Steyn, D. G., Watson, I. D., & Voogt, J. A. (1991). Simulation of surface urban heat islands under 'ideal' conditions at night. Part I: Theory and test against field data. *Boundary Layer Meteorology*, *56*, 275–294.

Kalkstein, L. S., & Davis, R. E. (1989). Weather and human mortality: An evaluation of demographic and interregional responses in the United States. *Annals of the Association of American Geographers*, *79*, 44–64.

Kim, Y., & Baik, J. (2002). Maximum urban heat island intensity in Seoul. *Journal of Applied Meteorology*, *41*, 651–659.

Klock, L., Zwart, S., Verhagen, H., & Mauri, E. (2012). The surface heat island of Rotterdam and its relationship with urban surface characteristics. *Resources, Conservation, and Recycling*, *64*, 23–29.

Klysik, K., & Fortuniak, K. (1999). Temporal and spatial characteristics of the urban heat island of Lodz, Poland. *Atmospheric Environment*, *33*, 38885–43895.

Lo, & Quattrochi. (2003). Land-use and land-cover change, urban heat island phenomenon, and health implications: Remote sensing approach. *Photogrammetric Engineering & Remote Sensing*, *69*(9), 1053–1063.

McPherson, G. E., Nowak, D., Heisler, G., Grimmond, S., Souch, C., Grant, R., et al. (1997). Quantifying urban forest structure, function, and value: The Chicago urban forest climate project. *Urban Ecosystems*, *1*, 49–61.

NWS Chicago Records. (2012). *Chicago region temperature records*. Retrieved from: http://www.crh.noaa.gov/lot/?n=chi_temperature_records

Oke, T. R. (1973). City size and the urban heat island. *Atmospheric Environment*, *7*(8), 769–779.

Oke, T. R. (1987). *Boundary layer climates*. Cambridge: University Press.

Oke, T. R. (1988). Street design and urban canopy layer climate. *Energy and Buildings*, *11*, 103–113.

Oke, T. R. (2004). *Initial guidance to obtain representative meteorological observations at urban sites No. 81*. World Meteorological Organization.

Oke, T. R. (2006). Towards better scientific communication in urban climate. *Theories of Applied Climatology*, *84*, 179–190.

Oke, T. R., Johnson, G. T., Steyn, D. G., & Watson, I. D. (1991). Simulation of surface urban heat islands under 'ideal' conditions at night––Part 2: Diagnosis and causation. *Boundary Layer Meteorology*, *56*, 339–358.

Onset HOBO data loggers. Retrieved from: http://www.onsetcomp.com/

Oswald, E. M., Rood, R. B., Zhang, K., Gronlund, C. J., O'Neill, M. S., White-Newsome, J. L., et al. (2012). An investigation into the spatial variability of near-surface air temperatures in the Detroit, Michigan, Metropolitan Region. *Journal of Applied Meteorology and Climatology*, *51*, 1290–1304.

Sakakibara, Y. (1996). A numerical study of the effect of urban geometry upon the surface energy budget. *Atmospheric Environment*, *30*(3), 487–496.

Santamouris, M. (2001). *Energy and climate in the urban built environment*. New York, NY: Routledge.
Shashua-Bar, I., & Hoffman, M. E. (2000). Vegetation as a climatic component in the design of an urban street: An empirical model for predicting the cooling effect of urban green areas with trees. *Energy and Buildings*, *31*, 221–235.
Sheridan, S. (2012). *Spatial synoptic classification system*. Retrieved from: http://sheridan.geog.kent.edu/ssc.html
Stathopoulou, M., & Cartalis, C. (2007). Daytime urban heat islands from Landsat ETM+ and Corine land cover data: An application to major cities in Greece. *Solar Energy*, *81*, 358–368.
Stempihar, J., Pourshams-Manzouri, T., Kaloush, K., & Rodezno, M. (2012). Porous asphalt pavement temperature effects for urban heat island analysis. *Transportation Research Record: Journal of the Transportation Research Board*, *2293*, 123–130.
Stewart, I. D. (2011). A systematic review and scientific critique of methodology in modern urban heat island literature. *International Journal of Climatology*, *31*, 200–217.
Stewart, I. D., & Oke, T. R. (2012). Local climate zones for urban temperature studies. *Bulletin of the American Meteorological Society*, *93*, 1879–1900.
Stone, B., Jr. (2012). *The city and the coming climate: Climate change in the places we live*. New York, NY: Cambridge University Press.
Stone, B., & Norman, J. M. (2006). Land use planning and surface heat island formation: A parcel-based radiation flux approach. *Atmospheric Environment*, *40*, 3561–3573.
Svensson, M. K. (2004). Sky view factor analysis – Implications for urban air temperature differences. *Meteorological Applications*, *11*, 201–211.
US Census. (2012). *Chicago 2010 US census population information*. Retrieved from: http://2010.census.gov/2010census/
$USGS_a$. (2012). *Earth explorer web tool*. Retrieved from: http://earthexplorer.usgs.gov/
$USGS_b$. (2012). *Elevations and distances in the United States*. Retrieved from: http://egsc.usgs.gov/isb/pubs/booklets/elvadist/elvadist.html#50
Vavrus, S., & Van Dorn, J. (2010). Projected future temperature and precipitation extremes in Chicago. *Journal of Great Lakes Research*, *36*, 22–32.
Voogt, J. A., & Oke, T. R. (2003). Thermal remote sensing of urban climates. *Remote Sensing of Environment*, *86*, 370–384.
Weng, Q. (2009). Thermal infrared remote sensing for urban climate and environmental studies: Methods, applications, and trends. *ISPRS Journal of Photogrammetry and Remote Sensing*, *64*, 335–344.
Weng, Q., & Quattrochi, D. A. (2006). Thermal remote sensing of urban areas: An introduction to the special issue. *Remote Sensing of Environment*, *104*, 119–122.